Influence of Channel Parameters on Noncoherent Massive MIMO Systems

Stephan Bucher[1], George Yammine[2], Robert F. H. Fischer[2], and Christian Waldschmidt[1]
[1]Institute of Microwave Engineering, [2]Institute of Communications Engineering
Ulm University, 89081 Ulm, Germany
Email: {stephan.bucher, george.yammine, robert.fischer, christian.waldschmidt}@uni-ulm.de

***Abstract*—In multi-user massive MIMO uplink systems, noncoherent detection schemes offer an appealing alternative to classical coherent detection algorithms. Sorted decision-feedback differential detection (DFDD) in combination with noncoherent decision-feedback equalization (nDFE) over the users have been demonstrated to achieve comparable results to the coherent case. Up to now, the assessment of noncoherent detection has been performed on the basis of an idealized channel model. In this paper, the influence of channel parameters on the performance of noncoherent massive MIMO systems is analyzed via an extensive simulation study. Thereby, a realistic channel model, in particular the COST 2100 channel model, forms the basis for the evaluation. It is shown that performance is highly dependent on the actual channel settings as well as on the power control of the transmitter. A further outcome is that the idealized channel model in previous studies ignores correlation effects and exhibits other power distributions among the receiving antennas. As a consequence, further optimization steps for noncoherent detection are required.**

I. Introduction

Multiple-input/multiple-output (MIMO) systems, where the base station is equipped with a very large number of receive antennas, so-called *massive MIMO*, have attracted growing attention, e.g., [1]–[3]. In order to exploit the benefits of massive MIMO, accurate channel knowledge is required at the base station. Channel estimates are usually obtained from pilot signals, which are transmitted by the users. As the number of channel coefficients is huge in massive MIMO systems, the estimation quickly becomes very challenging.

An attractive way to overcome the problem of requiring a large number of pilot symbols and to eliminate the need of channel estimation is to employ noncoherent detection. Based on the similarities between ultra-wideband (UWB) systems and the massive MIMO case, noncoherent detection schemes have been proposed in [4], [5] and assessed for a uniform linear array with omni-directional antennas as well as for antennas having a directional characteristic in [6]. However, up to now the performance evaluation has been based on an idealized, geometric channel model.

In this paper, the influence of channel parameters on the performance of noncoherent massive MIMO systems is analyzed. In contrast to previous studies, a cluster-based channel model, particularly the *COST 2100* channel model [7], [8], is employed. Besides new insights on the impact of the channel parameters, a power control of the transmitter is analyzed and a comparison to previous channel model is made.

This work was supported by Deutsche Forschungsgemeinschaft (DFG) under grant WA 3506/5-1.

The paper is organized as follows. In Sec. II, the system model and the COST 2100 channel model are introduced. Additionally, noncoherent detection in massive MIMO is briefly reviewed. Numerical results are presented and discussed in Sec. III including a comparison to the idealized channel model utilized in previous studies. Conclusions are drawn in Sec. IV.

II. System Model and Noncoherent Detection

Throughout this paper, a multi-user uplink scenario is considered (see Fig. 1). N_u single-antenna users simultaneously transmit to a central base station (BS), which is equipped with a very large number of receive antennas $N_\mathrm{rx} \gg N_\mathrm{u}$. The transmit symbols $b_{k,u}$ (user u at each discrete time step k) are drawn from an M-ary PSK constellation $\mathcal{M} = \{\mathrm{e}^{\mathrm{j}2\pi \cdot i/M} \mid i = 0, 1, \ldots, M-1\}$ and are differentially encoded afterwards. At the receiver, noncoherent detection methods based on the autocorrelation of the receive signal of different time steps are applied.

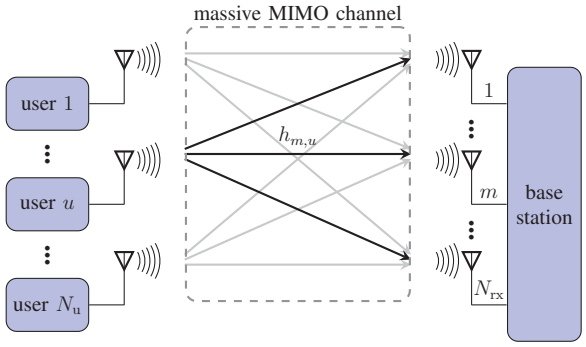

Fig. 1. Illustration of the multi-user massive MIMO uplink system.

A. COST 2100 MIMO Channel Model

The massive MIMO channel is modeled using a geometry-based stochastic approach, more precisely the COST 2100 channel model [7], [8]. This channel model can reproduce the stochastic properties of MIMO channels over time, frequency, and space. Essentially, this model bases its operation on placing clusters randomly in the topological simulation area. These clusters emulate physical scattering objects and consist of groups of multipath propagation components, which the

ISBN 978-3-8007-4541-8

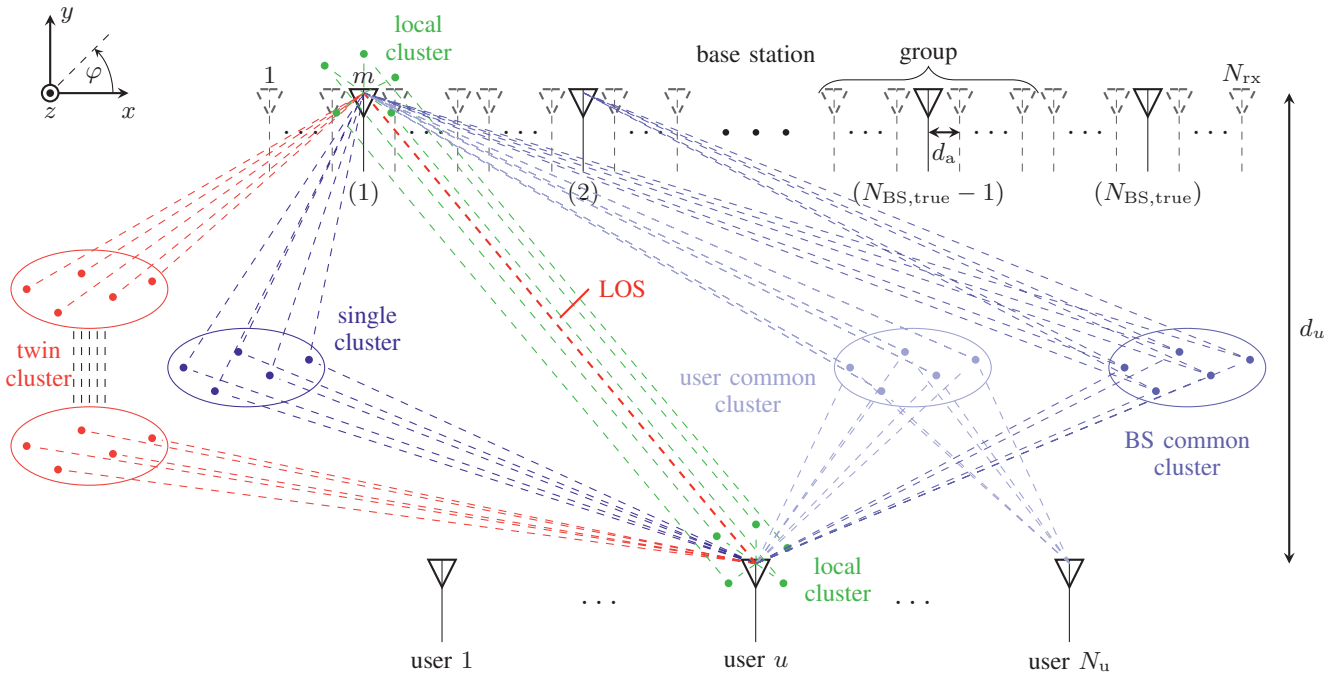

Fig. 2. Overview of the extended COST 2100 channel model for multi-user massive MIMO transmission. Depicted clusters are exemplary for user u and base station antenna m. True antennas are drawn in solid and interpolated antennas in dashed.

parameters thereof (such as direction and complex amplitude) are calculated on the basis of the geometry of the simulation region. Basically, there are three kinds of clusters in the COST 2100 model. On the one hand, there are local clusters covering the scenario, where scatterers surround users and base station. On the other hand, there are single and twin clusters distributed throughout the simulation area representing the scattering mechanism with one or multiple objects.

The time-variant and spatially-variant nature of the radio channel is modeled by introducing cluster *visibility regions (VR)*, which are circular regions of fixed size in the azimuth plane of the simulation area and control the activity of a particular cluster. Each cluster (except local clusters) is assigned to at least one VR and is activated only when the user enters the corresponding VR.

The COST 2100 model initially assumes conventional MIMO systems using small and compact arrays. Unlike conventional MIMO, antenna arrays of massive MIMO systems equipped with a large number of antennas can span hundreds of wavelengths in space. Due to this fact, the plane wave assumption does not hold and spherical wavefronts are observed. Consequently, the propagation channel cannot be seen as wide-sense stationary [9]. In order to support physically large arrays and model the spatial variation at the base station, all BS antennas or groups of them representing a small MIMO array are placed in the topological simulation area. In [10], [11] the concept of visibility regions is extended to the BS side to capture the situation that several neighboring BS antennas share the same set of clusters. This extension is not considered in the current simulation framework so far. Instead, the concept of *common clusters* is applied, which has been proposed to support multi-link simulations and to address inter-link correlation [12], [13]. Thus, several BS antennas see the same cluster (BS common clusters) but independent of their location. This approach is also done at user side, where a certain portion of the energy of different users propagate through the same cluster (user common clusters). Besides multipath propagation, also direct propagation (line-of-sight, LOS) from user to base station can be taken into account.

An overview of the multi-user massive MIMO channel model comprising all aspects as described above is depicted in Fig. 2. Users are arranged along a straight line in x-direction at a distance d_u to the base station. At the receiver a uniform linear array along the x-axis consisting of N_{rx} receive antennas with inter-element distance of d_{a} is assumed. As mentioned previously, all BS antennas or groups representing a small part of the receiver array can be placed in the topological simulation area. In the latter case, the midantenna of each group (indicated by solid lines) is actually placed, whereas the remaining antennas of each group (indicated by dash lines) are not positioned (their received signal is interpolated afterwards). The number of true (actually placed) BS antennas is denoted by $N_{\mathrm{BS,true}} \leq N_{\mathrm{rx}}$. All users as well as the base station are assumed to be at the same height and located in the azimuth plane. All kinds of clusters are depicted exemplarily for user u and BS antenna m.

The channel coefficient $h_{m,u}$ of each user u and a BS antenna m can be expressed as the sum of the complex amplitude of the LOS component $a_{m,u}^{\mathrm{LOS}}$ and all complex amplitudes of the multipath components $a_{i,m,u}^{\mathrm{MPC}}$ caused by clusters, which are visible for the respective user. Assuming omni-directional antennas at the user side and taking into

ISBN 978-3-8007-4541-8

account a directional antenna pattern $C_{\mathrm{rx}}(\varphi,\theta)$ at the BS side, the channel coefficients are given by

$$h_{m,u} = a_{m,u}^{\mathrm{LOS}}\, C_{\mathrm{rx}}(\varphi_{m,u}^{\mathrm{LOS}},\theta_{m,u}^{\mathrm{LOS}}) + \sum_i a_{i,m,u}^{\mathrm{MPC}}\, C_{\mathrm{rx}}(\varphi_{i,m,u}^{\mathrm{MPC}},\theta_{i,m,u}^{\mathrm{MPC}})\,, \tag{1}$$

where the direction of arrival (DOA) of the LOS component and the i-th multipath component are denoted by $\varphi_{m,u}^{\mathrm{LOS}}$ and $\theta_{m,u}^{\mathrm{LOS}}$, and by $\varphi_{i,m,u}^{\mathrm{MPC}}$ and $\theta_{i,m,u}^{\mathrm{MPC}}$, respectively. The complex amplitude of both the LOS component and the multipath component depend on the length of the propagation path $d_{m,u}^{\mathrm{LOS}}$ and $d_{i,m,u}^{\mathrm{MPC}}$ according to

$$a_{m,u}^{\mathrm{LOS}} \sim \frac{1}{f_{\mathrm{c}}\, d_{m,u}^{\mathrm{LOS}}} \mathrm{e}^{-\mathrm{j}kd_{m,u}^{\mathrm{LOS}}}\,, \tag{2}$$

$$a_{i,m,u}^{\mathrm{MPC}} \sim \frac{1}{f_{\mathrm{c}}\, d_{i,m,u}^{\mathrm{MPC}}} \mathrm{e}^{-\mathrm{j}kd_{i,m,u}^{\mathrm{MPC}}}\,, \tag{3}$$

where $k = 2\pi/\lambda$ is the wavenumber, λ is the wavelength, and f_{c} denotes the operating frequency. The ratio in (2) and (3) describes the path loss, whereas the remaining term ($\mathrm{e}^{-\mathrm{j}\{\cdot\}}$) is the change in phase. Since clusters are randomly distributed throughout the simulation area and the multipath components within local clusters follow a uniform distribution and within single/twin/common clusters a Gaussian distribution, the length of the propagation path $d_{i,m,u}^{\mathrm{MPC}}$ in (3) becomes random for different channel realizations. In contrast, the LOS component is deterministic as $d_{m,u}^{\mathrm{LOS}}$ in (2) is constant.

Equation (1) holds, when all BS antennas are placed in the simulation area ($N_{\mathrm{BS,true}} = N_{\mathrm{rx}}$). Otherwise channel coefficients of interpolated antennas are generated by means of steering vectors and on the basis of the received signal at the true BS antenna, i.e., on the given complex amplitudes. As a physical small part of the entire linear array is considered, a plane wave and small bandwidth assumption is applied and the expected receive signal of LOS and each multipath component is recovered according to their DOA [14]. For instance, if the number of group members amounts to N_{group}, the complex amplitude of the i-th multipath component of the n-th member of the m-th antenna group is reconstructed as follows

$$a_{i,n_{\mathrm{group},m},u}^{\mathrm{MPC}} = a_{i,m_{\mathrm{true}},u}^{\mathrm{MPC}}\, \mathrm{e}^{\mathrm{j}k\left(n-\frac{N_{\mathrm{group}}+1}{2}\right)d_{\mathrm{a}}\cos\left(\varphi_{i,m_{\mathrm{true}},u}^{\mathrm{MPC}}\right)}\,. \tag{4}$$

The same approach is applied to the LOS component. An amplitude compensation due to path losses is not considered.

B. Noncoherent Detection

Assuming the channel coefficients $h_{m,u}$ to be constant over a burst of N_{bl} symbols, the receiving block $\boldsymbol{R}$ over N_{bl} time steps and N_{rx} receive antennas is given by

$$\boldsymbol{R} = \boldsymbol{H}\boldsymbol{B} + \boldsymbol{N}\,, \tag{5}$$

where the matrix $\boldsymbol{H} \overset{\text{def}}{=} [\boldsymbol{h}_1,\ldots,\boldsymbol{h}_{N_{\mathrm{u}}}]$ contains the (column) channel coefficient vectors $\boldsymbol{h}_u \overset{\text{def}}{=} [h_{1,u},\ldots,h_{N_{\mathrm{rx}},u}]^{\mathsf{T}}$ and the matrix $\boldsymbol{B} \overset{\text{def}}{=} [\boldsymbol{b}_1^{\mathsf{T}},\ldots,\boldsymbol{b}_{N_{\mathrm{u}}}^{\mathsf{T}}]^{\mathsf{T}}$ consists of the (row) vectors $\boldsymbol{b}_u \overset{\text{def}}{=} [b_{0,u},\ldots,b_{N_{\mathsf{bl}},u}]$ of transmit symbols of each user u, respectively. The matrix $\boldsymbol{N}$ collects the circular-symmetric zero-mean complex Gaussian noise $n_{m,k}$ with variance σ_{n}^2.

In view of block processing, *multiple-symbol differential detection (MSDD)* or its reduced-complexity version *decision-feedback differential detection (DFDD)* is applied [4]. Differential detection of the symbols of user u by means of the DFDD is based on the $N_{\mathsf{bl}} \times N_{\mathsf{bl}}$ *correlation matrix*

$$\boldsymbol{Z}_u \overset{\text{def}}{=} \boldsymbol{R}^H \boldsymbol{W}_u \boldsymbol{R}\,, \tag{6}$$

where $\boldsymbol{W}_u \overset{\text{def}}{=} \mathbf{diag}(w_{1,u},\ldots,w_{1,N_{\mathrm{rx}}})$ is the user-specific diagonal weighting matrix or user-specific window. This window provides means of separating the different users in the spatial domain and is linked to the power distribution of each user among the receive antennas, i.e., power-space profile (PSP). The PSP can be obtained from averaging over different channel realizations according to

$$P_{m,u} \overset{\text{def}}{=} \mathrm{E}\{|h_{m,u}|^2\}\,. \tag{7}$$

Performance improvements can be achieved by applying *noncoherent decision-feedback equalization (nDFE)* over the users [5]. The main idea behind nDFE is the subtraction of the average interference caused by the already detected users. In contrast to coherent interference cancellation techniques (such as BLAST [15]) where actual channel knowledge is required, nDFE operates based on the statistics about the channel coefficients (PSP) and not the channel coefficients themselves.

III. Simulation Results

A. Influence of Channel Parameters

Simulations are conducted for an $N_{\mathrm{u}} = 3$ user scenario, where the base station is equipped with a uniform linear array consisting of $N_{\mathrm{rx}} = 100$ antennas (see Fig. 2). First, a reference scenario is defined. Then, the channel parameters, in particular user distance d_u, antenna distance d_{a}, kinds of clusters and true number of BS antennas $N_{\mathrm{BS,true}}$ are modified covering their influence.

As a starting point, an indoor hall environment is assumed, where no direct path between user and base station is present. Hence, no LOS component exists. The relevant parameterization of the COST 2100 channel model for this scenario is taken from [8], where measurement campaigns at 5 GHz have been carried out and parameters of respective clusters have been extracted. In the defined scenario, all kinds of clusters are active, except single clusters. The base station is positioned in the center of the coordinate system along the x-axis using an inter-element distance of one wavelength ($d_{\mathrm{a}} = \lambda$). The operating frequency is set to $f_{\mathrm{c}} = 1\,\mathrm{GHz}$, which leads to a physically large array at the base station spanning 30 m. Users are placed at a distance of $d_u = 5\,\mathrm{m}$ in front of the receiver, where the x-position of user 1 and 3 equals that of BS antenna 20 and 80, respectively. The x-position of user 2 is varied. In the first instance, 20 true base station antennas ($N_{\mathrm{BS,true}} = 20$) of 100 in total are positioned in the simulation area. Each true antenna represents a group of five receive antennas. Achieving

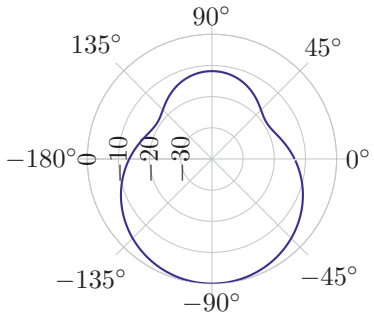

Fig. 3. Azimuth radiation pattern $C_{\mathrm{rx}}(\varphi, \theta = 90°)$ (in dB) of a patch antenna utilized at the base station side. Main lobe is directed towards the users.

better user separation regarding the PSP, the antennas at the base station should exhibit some directional characteristics [6]. Therefore, a patch antenna is chosen, whose radiation pattern in the azimuth plane is shown in Fig. 3. Its main lobe is directed in negative y-direction towards the users.

The performance measure is the symbol-error rate (SER) as function of the x-position of user 2. To this end, 10000 channel realizations are generated for each x-position of user 2 within a specified range. During the acquisition of the different channel realizations, none of the users is moving, i.e., a static scenario is considered. Afterwards, noncoherent detection is performed either via DFDD or via DFDD/nDFE. The transmit symbols of each user are 4PSK symbols, which are differentially encoded, and the block length amounts to $N_{\mathrm{bl}} = 200$. The noise power is fixed in such a way that the ratio of the symbol energy E_{s} and the noise power spectral density N_0 (signal-to-noise ratio, SNR) amounts to 14 dB. The PSP is extracted from the channel coefficients according to (7) and is normalized for an average total receive power of one for each user. For the same purpose, a normalization is applied to the channel matrix particular to the channel columns, where $||\boldsymbol{h}_u||_2^2 = 1$. Parameters of the COST 2100 channel model and for noncoherent detection are summarized in Table I.

The results are depicted in Fig. 4a, where the SER is plotted for each user individually. It can be observed, when user 2 is positioned too close to user 1 or 3, a performance degradation of the said users occurs. This observation has already been made in [5] and is caused by a high overlap of the PSPs. The respective power profile of each user is shown in Fig. 4a, where user 2 is centered between the other users regarding the x-position. The profiles exhibit a stepped characteristic, which is due to the fact that only phases are reconstructed of the interpolated BS antennas and no amplitude correction due to path losses is considered, i.e., the power remains constant within one BS group. Applying DFDD leads to a poor performance for user 2 due to the high interference of the other users. This interference can be lowered by means of nDFE, which obtains substantial gains. In order to provide a basis for performance comparison, results when applying BLAST with perfect channel knowledge is illustrated as well in Fig. 4a. It is apparent, that a difference in performance between noncoherent and coherent detection is present in current scenario. However, this comparison should be treated with caution as no estimation error for BLAST is taken into account (cf. fair comparison in [16]).

TABLE I
PARAMETERIZATION OF COST 2100 CHANNEL MODEL AND NONCOHERENT DETECTION FOR REFERENCE SCENARIO

COST 2100 channel model	
number of users N_{u}	3
user distance d_u	5 m
number of true BS antennas $N_{\mathrm{BS,true}}$	20
total number of BS antennas N_{rx}	100
operating frequency f_{c}	1 GHz
BS antenna spacing d_{a}	λ
type of BS antenna	patch
kinds of clusters	common, twin, local
Noncoherent detection	
modulation alphabet	4-ary DPSK
block length N_{bl}	200
SNR E_{s}/N_0	14 dB
channel normalization (power control)	$\|\|\boldsymbol{h}_u\|\|_2^2 = 1$
PSP normalization	$\sum_{m=1}^{N_{\mathrm{rx}}} P_{m,u} = 1$

In the following, several channel parameters shall be modified to determine their impact. Note that only one parameter (unless stated otherwise) of the initial scenario is changed.

1) User distance: First, the user distance is varied. Fig. 4b shows the results for SER and PSP, when d_u is increased to 10 m. Increasing the user distance broadens the power-space profile as the path loss difference among the propagation paths between user and each BS antenna is lowered and less impact of the receive antenna pattern occurs due to a shrinked DOA range. In turn, broadening of the PSP leads to a higher overlap of the individual PSPs and decreases the user separability. Consequently, the SER using noncoherent detection gets worse due to higher user interferences. For coherent detection using BLAST a slight improvement is noticeable. Due to the power-defocusing effect (broad PSP), almost all BS antennas contribute to the overall system leading to a gain in diversity order.

2) Antenna spacing: Second, the impact of inter-element spacing of the base station antennas is investigated. For this purpose, d_{a} is halved to $\lambda/2$, which also shrinks the receiving array by a factor of two spanning now 15 m. In order to keep the comparison fair, the studied x-position range is halved in the same manner. In this case, almost the same behavior can be observed compared to increasing the user distance (see Fig. 4c). Due to the reduced range of the base station, lower path losses and less impact of the BS pattern on the receive power occur resulting in broad PSPs. Higher user interference caused by increased overlapping of the individual PSPs deteriorates the SER. Once more, for coherent detection using BLAST a slight improvement is observable originated from a gain in diversity order as in Sec. III-A1.

3) Kinds of clusters: Next, the influence of the existence of different kinds of clusters on the system performance is studied. In the starting scenario all kinds of clusters except

ISBN 978-3-8007-4541-8

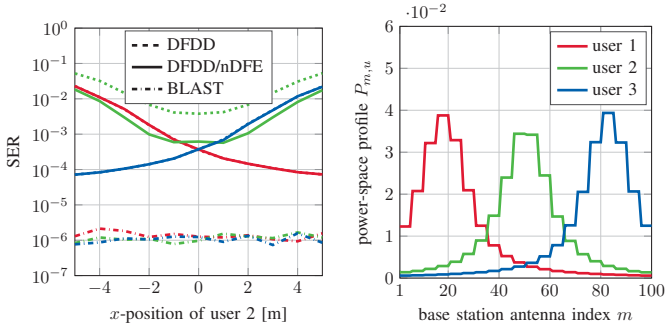

(a) Parameterization according to Table I.

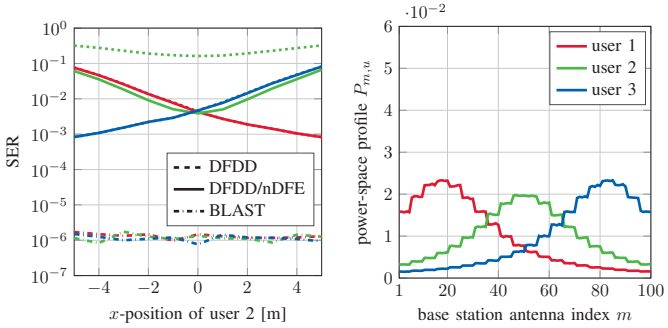

(b) User distance increased to $d_u = 10\,\mathrm{m}$.

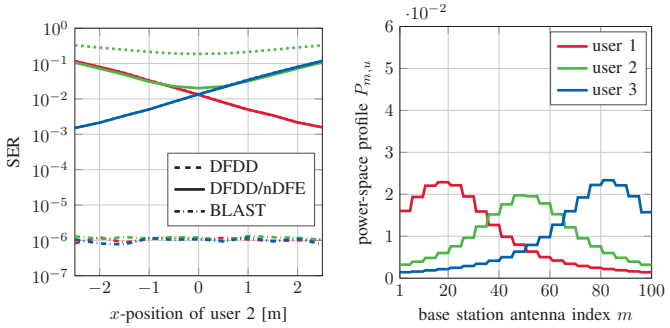

(c) Antenna distance decreased to $d_\mathrm{a} = \lambda/2$.

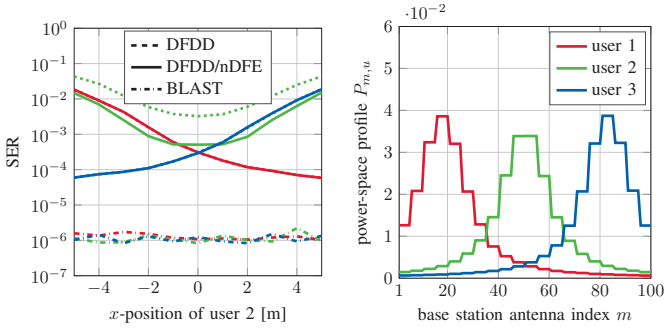

(d) Common clusters deactivated.

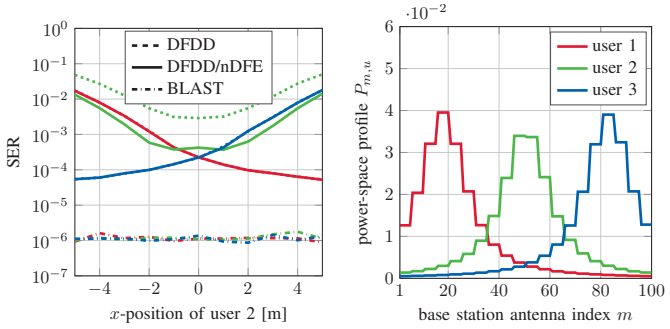

(e) Only local clusters activated.

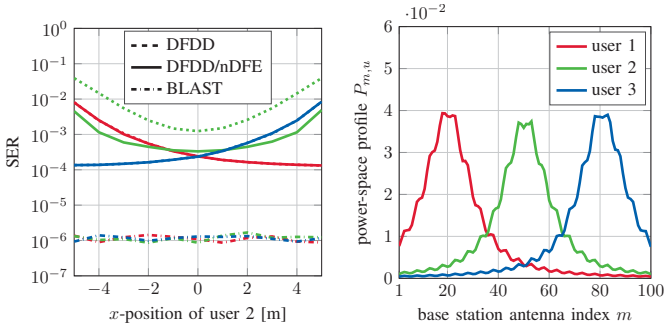

(f) $N_{\mathrm{BS,true}} = 100$ and only local clusters (distributed around a group of five BS antennas) activated.

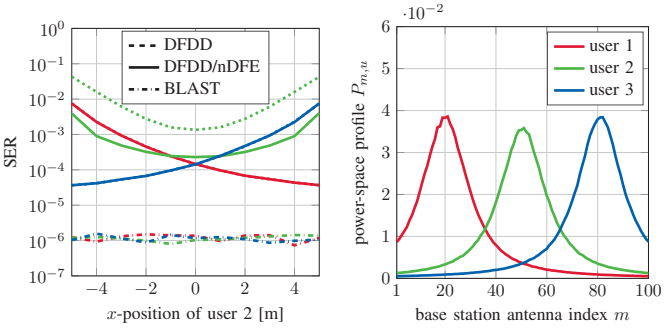

(g) $N_{\mathrm{BS,true}} = 100$ and only local clusters (independent for each BS antenna) activated.

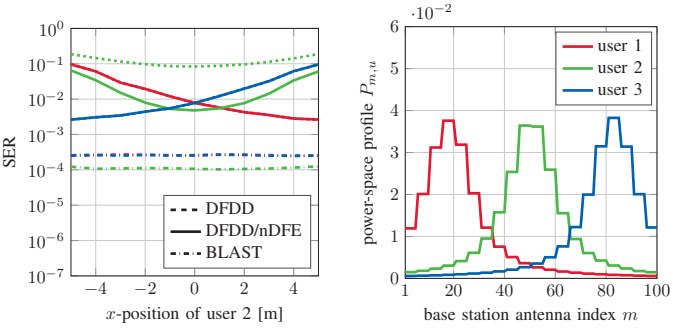

(h) Channel and power-space profile normalized to $||\mathbf{H}||_\mathrm{F}^2 = N_\mathrm{u}$ and $\sum_{u=1}^{N_u} \sum_{m=1}^{N_\mathrm{rx}} P_{m,u} = N_\mathrm{u}$, respectively.

Fig. 4. Symbol error rate vs. x-position of user 2 (colors correspond to users: user 1 (—), user 2 (—), user 3 (—)) and power-space profile at zero x-position of user 2. Parameterization according to Table I.

ISBN 978-3-8007-4541-8

single clusters were activated. In the first instance, common clusters (BS and user) are disabled (see Fig. 4d) and afterwards twin clusters are deactivated as well such that only local clusters remain (see Fig. 4e). In both cases no remarkable changes are observable in the PSPs. Regarding the SER, performance improvements are achieved, especially when only local clusters are present. Exclusion of common clusters primarily reduces the correlation of the received signals. The same applies, when only local clusters are active.

4) Number of true BS antennas: Finally, the role of the number of true BS antennas is treated. Now, all BS antennas are placed in the simulation area ($N_{\mathrm{BS,true}} = N_{\mathrm{rx}}$) and the focus is set on situation in Sec. III-A3, where only local clusters are activated. It is necessary to distinguish between two scenarios. First, a group of receiving antennas see the same local clusters, which are distributed around the midantenna (as in Sec. III-A3). Second, each BS antenna has its own independent local clusters. The results of these cases are depicted in Figs. 4f and 4g, respectively. Since both the phase and the amplitude of the channel coefficients are calculated for each BS antenna according to (1), the power-space profiles do not exhibit a stepped characteristic anymore. Compared to the reference scenario, almost no influence on the system performance is observed regarding the zero x-position of user 2. However, the change in SER is smaller when the x-position is varied originating from the smoothed PSPs. In the second case, SER is further improved, which results from lower correlation of the received signals due to independent local clusters at each BS antenna.

In conclusion, different distances (d_{u}, d_{a}) and the type of clusters in use influence the power-space profile as well as the correlation of the received signals and thus affect the performance of noncoherent detection. The best outcome is obtained where the antenna spacing is large, the user distance is moderate and only independent local clusters arise in the propagation environment. Usually, the set of clusters is fixed in a given scenario and consequently only the physical dimensions remain for optimization.

B. Power Control

Besides the parameters discussed above, power control of the transmitters is another important issue. In the reference scenario, the channel matrix as well as the power-space profile are normalized in such a way that the power of each user would be one. This approach regards no power variation among the users, which can occur due to the different positioning in front of the receiving array. In order to include variations between the users, but to eliminate the overall fading effects, a power control is analyzed, where the total received power is scaled to the number of users N_{u}, i.e., $||\mathbf{H}||_{\mathrm{F}}^2 = N_{\mathrm{u}}$, where $||\cdot||_{\mathrm{F}}$ denotes the Frobenius norm and $\sum_{u=1}^{N_u}\sum_{m=1}^{N_{\mathrm{rx}}} P_{m,u} = N_{\mathrm{u}}$, respectively. Applying this regulation on the initial scenario as in Sec. III-A, a general performance loss of both, noncoherent detection and BLAST, can be observed comparing the SER at zero x-position of user 2 (see Fig. 4h). However, the difference in performance between

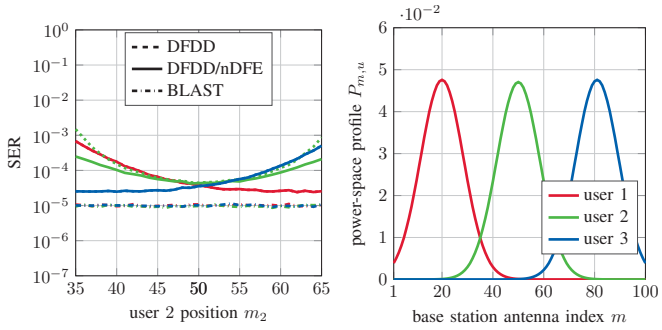

(a) (b)

Fig. 5. (a) Symbol error rate vs. user 2 position m_2 using idealized channel model in [6] (colors correspond to users: user 1 (—), user 2 (—), user 3 (—)) and (b) power-space profile at $m_2 = 50$. Parameterization adapted to Table I of COST 2100 channel model evaluation, $\gamma = 3.6$ and $\zeta^2 = 77$.

coherent and noncoherent detection is slightly reduced. In addition, as the receive power of each user is not adjusted individually but jointly (PSP exhibit almost the same height in Fig. 4h), SER of user 2 is improved due to the higher receive power.

C. Comparison to Idealized Channel Model

In previous studies ([4], [6]), noncoherent detection has been assessed by means of an idealized and geometric channel model, where also a uniform linear array (antenna spacing d_{a}) has been assumed. Users are placed along a straight line in front of the array (user distance d_u) and a pure path-loss model (exponent γ) is applied. The user specific power-space profile can be approximated by

$$P_{m,u} \overset{\mathrm{def}}{=} \mathrm{E}\left\{|h_{m,u}|^2\right\} \approx c_{\mathrm{p}}\, \mathrm{e}^{-\frac{|m-m_u|^2}{(2\zeta^2)}}\, |C_{\mathrm{rx}}(\varphi_{m,u})|^2\,, \qquad (8)$$

where m_u denotes the antenna element closest to the user u and $\zeta^2 = d_u^2/(d_{\mathrm{a}}^2\gamma)$. The receive antenna pattern is taken into account by $C_{\mathrm{rx}}(\varphi_{m,u})$, where $\varphi_{m,u}$ is the angle under which the user u is seen at the array by BS antenna m. The normalization constant c_{p} guarantees an average total receive power of one for each user. The channel coefficients are generated by means of the power-space profile. To be more precise, they are independent of each other and are zero-mean, circular-symmetric complex Gaussian random variables with variance according to the PSP. This approach creates uncorrelated channels and considers local scatterers only.

In order to enable a direct comparison of the idealized and the COST 2100 channel model, parameters are adapted appropriately to capture the scenario as in Sec. III-A. In particular, the distances (d_u, d_{a}) as well as the BS receive pattern and the parameters for noncoherent detection are chosen according to Table I. The same applies to the user positioning, where user 1 and 3 are in front of BS antenna 20 and 80, respectively. As in [6], the path loss exponent is set to 3.6 resulting in $\zeta^2 = 77$. The position of user 2 is again varied parallel to the receiving array and SER is plotted as function of the BS antenna index m_2, which user 2 is closest to (instead of the absolute x-position). The result is averaged over 300000

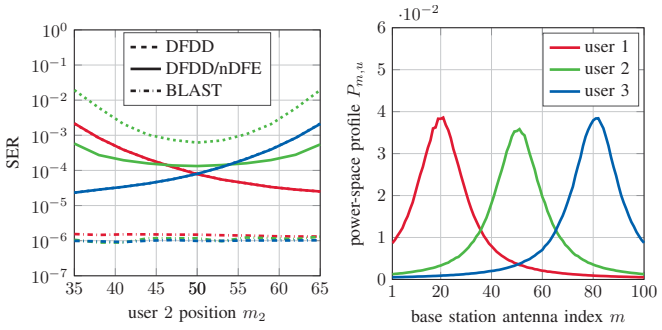

(a) (b)

Fig. 6. (a) Symbol error rate vs. user 2 position m_2 using idealized channel model in [6] (colors correspond to users: user 1 (—), user 2 (—), user 3 (—)) and (b) power-space profile at $m_2 = 50$, which is taken from the COST 2100 channel model evaluation of Fig. 4g.

channel realizations and is illustrated in Fig. 5. Comparing the results to Fig. 4g from the COST 2100 model, where only local clusters are activated, a significant performance gain can be noted. This can be explained by the following fact. The users' PSPs exhibit a distinctly narrower shape resulting in less user interferences in noncoherent detection. Furthermore, BLAST performance is worse, which is due to the lower number of effective antennas the received power is induced on, and leads to almost the same performance of coherent and noncoherent detection. Taking into account estimation errors, the noncoherent scheme may even outperform the coherent one in this case. Consequently, the idealized channel model does not produce equivalent PSPs, when parameters are adapted to the scenario of the COST 2100 channel model. For a fair comparison and in order to exclude further effects, the performance is tested using the same PSPs of the COST 2100 channel model evaluation in Fig. 4g for the idealized channel model. The result is depicted in Fig. 6. Despite that the same PSPs are utilized, the overall SER is slightly improved compared to Fig. 4g. This is due to the fact that the channel coefficients are generated independently, thus no correlation of the received signals is taken into account. Hence, given the correct PSPs and considering local clusters only, the idealized channel model can produce comparable results as the COST 2100 channel model. In other words, the COST 2100 channel model is a comprehensive model, where many aspects of any given scenario can be controlled and simulated. However, it is computationally expensive. In the case where the PSPs are known beforehand, and channel correlation information is not required, the idealized channel model is a good lower complexity approximation.

IV. Conclusion

In this paper, noncoherent detection in multi-user massive MIMO systems has been investigated by means of a cluster-based channel model, more specifically the COST 2100 channel model. It has been shown that the channel parameters like physical distances and the set of clusters in the simulation environment influence the performance significantly. Furthermore, the power control of the transmitter has to be adapted when a distinction of the power distribution of the individual users among the receiving array is needed. A comparison to previous studies, where the assessment has been based on an idealized channel model, revealed a substantial performance loss. This originated from no consideration of any correlation and other power distributions of the users among the receive antennas leading to excessively optimistic results. Consequently, further optimization steps have to be performed to improve the performance of noncoherent detection, where one task could be narrowing the power-space profiles. This aim can be accomplished by enlarging the inter-element distance at the BS side or by highly directional antennas.

References

[1] F. Rusek, D. Persson, B. K. Lau, E. G. Larsson, T. L. Marzetta, O. Edfors, and F. Tufvesson, "Scaling Up MIMO: Opportunities and Challenges with Very Large Arrays," *IEEE Signal Processing Magazine*, vol. 30, no. 1, pp. 40–60, Jan. 2013.

[2] E. G. Larsson, O. Edfors, F. Tufvesson, and T. L. Marzetta, "Massive MIMO for Next Generation Wireless Systems," *IEEE Communications Magazine*, vol. 52, no. 2, pp. 186–195, Feb. 2014.

[3] S. Yang and L. Hanzo, "Fifty Years of MIMO Detection: The Road to Large-Scale MIMOs," *IEEE Communications Surveys & Tutorials*, vol. 17, no. 4, pp. 1941–1988, 2015.

[4] A. Schenk and R. F. H. Fischer, "Noncoherent Detection in Massive MIMO Systems," in *17th International ITG Workshop on Smart Antennas (WSA)*, Mar. 2013, pp. 1–8.

[5] R. F. H. Fischer and M. Bense, "Noncoherent Decision-Feedback Equalization in Massive MIMO Systems," in *International Zurich Seminar on Communications (IZS)*, Feb. 2014, pp. 112–115.

[6] G. Yammine, R. F. H. Fischer, and C. Waldschmidt, "On the Influence of the Antenna Pattern in Noncoherent Massive MIMO Systems," in *International Symposium on Wireless Communication Systems (ISWCS)*, Aug. 2015, pp. 391–395.

[7] L. Liu, C. Oestges, J. Poutanen, K. Haneda, P. Vainikainen, F. Quitin, F. Tufvesson, and P. D. Doncker, "The COST 2100 MIMO Channel Model," *IEEE Wireless Communications*, vol. 19, no. 6, pp. 92–99, Dec. 2012.

[8] R. Verdone and A. Zanella, Eds., *Pervasive Mobile and Ambient Wireless Communications*. Springer London, 2012.

[9] X. Li, S. Zhou, E. Björnson, and J. Wang, "Capacity Analysis for Spatially Non-Wide Sense Stationary Uplink Massive MIMO Systems," *IEEE Transactions on Wireless Communications*, vol. 14, no. 12, pp. 7044–7056, Dec. 2015.

[10] X. Gao, F. Tufvesson, and O. Edfors, "Massive MIMO channels — Measurements and Models," in *Asilomar Conference on Signals, Systems and Computers*, Nov. 2013, pp. 280–284.

[11] X. Gao, J. Flordelis, G. Dahman, F. Tufvesson, and O. Edfors, "Massive MIMO Channel Modeling - Extension of the COST 2100 Model," in *Joint NEWCOM/COST Workshop on Wireless Communications (JNCW)*, 2015.

[12] J. Poutanen, F. Tufvesson, K. Haneda, V. M. Kolmonen, and P. Vainikainen, "Multi-Link MIMO Channel Modeling Using Geometry-Based Approach," *IEEE Transactions on Antennas and Propagation*, vol. 60, no. 2, pp. 587–596, Feb. 2012.

[13] K. Haneda, J. Poutanen, F. Tuvfesson, L. Liu, V. M. Kolmonen, P. Vainikainen, and C. Oestges, "Development of Multi-Link Geometry-Based Stochastic Channel Models," in *Loughborough Antennas & Propagation Conference*, Nov. 2011, pp. 1–7.

[14] H. Krim and M. Viberg, "Two Decades of Array Signal Processing Research: the Parametric Approach," *IEEE Signal Processing Magazine*, vol. 13, no. 4, pp. 67–94, Jul. 1996.

[15] G. J. Foschini, D. Chizhik, M. J. Gans, C. Papadias, and R. A. Valenzuela, "Analysis and Performance of Some Basic Space-Time Architectures," *IEEE Journal on Selected Areas in Communications*, vol. 21, no. 3, pp. 303–320, Apr. 2003.

[16] R. F. H. Fischer, M. Bense, and C. Stierstorfer, "Noncoherent Joint Decision-Feedback Detection in Multi-User Massive MIMO Systems," in *18th International ITG Workshop on Smart Antennas (WSA)*, March 2014, pp. 1–8.

ISBN 978-3-8007-4541-8